AMERICAN SOCIETY FOR MICROBIOLOGY | Applied and Environmental Microbiology®

ENVIRONMENTAL MICROBIOLOGY

Molecular Adaptations of Bacterial Mercuric Reductase to the Hypersaline Kebrit Deep in the Red Sea

Eman Ramadan,[a]* Mohamad Maged,[a]* Ahmed El Hosseiny,[a] Felipe S. Chambergo,[b] João C. Setubal,[c] Hamza El Dorry[a]

[a]Department of Biology, School of Sciences and Engineering, The American University in Cairo, New Cairo, Egypt
[b]Escola de Artes Ciências e Humanidades, Universidade de São Paulo, São Paulo, Brazil
[c]Instituto de Química, Universidade de São Paulo, São Paulo, Brazil

ABSTRACT The hypersaline Kebrit Deep brine pool in the Red Sea is characterized by high levels of toxic heavy metals. Here, we describe two structurally related mercuric reductases (MerAs) from this site which were expressed in *Escherichia coli*. Sequence similarities suggest that both genes are derived from proteobacteria, most likely the *Betaproteobacteria* or *Gammaproteobacteria*. We show that one of the enzymes (K35NH) is strongly inhibited by NaCl, while the other (K09H) is activated in a NaCl-dependent manner. We infer from this difference that the two forms might support the detoxification of mercury in bacterial microorganisms that employ the compatible solutes and salt-in strategies, respectively. Three-dimensional structure modeling shows that all amino acid substitutions unique to each type are located outside the domain responsible for formation of the active MerA homodimer, and the vast majority of these are found on the surface of the molecule. Moreover, K09H exhibits the predominance of acidic over hydrophobic side chains that is typical of halophilic salt-dependent proteins. These findings enhance our understanding of how selection pressures imposed by two environmental stressors have endowed MerA enzymes with catalytic properties that can potentially function in microorganisms that utilize distinct mechanisms for osmotic balance in hypersaline environments.

IMPORTANCE Analysis of two structurally homologous but catalytically distinct mercuric reductases from the Kebrit Deep brine in the Red Sea sheds light on the adaptations that enable microorganisms to cope simultaneously with extreme salinity and toxic mercury compounds. One is strongly inhibited by high NaCl concentrations, while the other exhibits NaCl-dependent activation. Their different activity profiles imply that they may derive from bacterial microorganisms that utilize compatible solutes and salt-in strategies, respectively, to maintain osmotic balance. Three-dimensional modeling reveals that regions not involved in formation of the active homodimer are conserved between the two. However, in the NaCl-dependent form, distinct amino acid substitutions are found in areas that are critical for stability in high salt. The work provides insights into how two environmental stressors have shaped the structure of orthologous enzymes through selection and adaptation, enabling them to retain their catalytic function in what may be very different cellular contexts.

KEYWORDS Atlantis II Deep, Kebrit Deep, mercuric reductase, Red Sea brine pools

The vast diversity of environments found on our planet encompasses a range of ecosystems characterized by quite extreme physicochemical conditions. Examples of such environments are found in the oceans, in which levels of sunlight, oxygen, temperature, and salinity vary widely. The brine pools in the Red Sea provide an excellent example of the extreme conditions to be found in marine environments.

Citation Ramadan E, Maged M, El Hosseiny A, Chambergo FS, Setubal JC, El Dorry H. 2019. Molecular adaptations of bacterial mercuric reductase to the hypersaline Kebrit Deep in the Red Sea. Appl Environ Microbiol 85:e01431-18. https://doi.org/10.1128/AEM.01431-18.

Editor Emma R. Master, University of Toronto

Copyright © 2019 American Society for Microbiology. All Rights Reserved.

Address correspondence to Hamza El Dorry, hadorry@yahoo.com.

* Present address: Eman Ramadan, Faculty of Pharmacy, Department of Pharmacology and Biochemistry, the British University in Egypt, El-Sherouk City, Egypt; Mohamad Maged, Faculty of Biotechnology, October University for Modern Sciences and Arts, 6th of October City, Cairo, Egypt.

Received 2 July 2018
Accepted 20 November 2018
Accepted manuscript posted online 30 November 2018
Published 6 February 2019

Downloaded from http://aem.asm.org/ on August 29, 2020 by guest

Around 25 brine-filled deeps have been located along the central axis of the Red Sea (1), of which Atlantis II and Kebrit are the best studied (2–5). The Atlantis II and Kebrit brines are located in the central Red Sea (21°20.72′N and 38°04.59′E) and in the northern Red Sea (24°44′N and 36°17′E) at maximum depths of around 2,194 m and 1,549 m, respectively (1). Each of these hypersaline pools exhibits a unique set of physicochemical features. The lowest layers of Atlantis II and Kebrit exhibit salinities of around 26%, a pH of approximately 5.5, and extremely low levels of oxygen. However, they differ sharply in temperature, with maxima of 68.2°C at Atlantis II and 23.3°C at Kebrit (2–5). Both brines have high concentrations of heavy metals, but in contrast to Atlantis II, Kebrit is also characterized by remarkably high concentrations of H_2S (3).

The microbial communities found in these environments are exposed to multiple abiotic stressors, including toxic heavy metals, like mercury, and extremely high salinities, which approach saturation level (2–4, 6). To survive under these conditions, microbial communities in both brines must have evolved detoxification systems for mercury that are functional in the presence of high salt concentrations.

The enzyme mercuric reductase (MerA) is a central component of the mercury detoxification systems used by microorganisms that live in environments contaminated with toxic mercury compounds (7, 8). The flavoprotein MerA is a homodimeric oxidoreductase that catalyzes the reduction of the toxic ionic form of mercury (Hg^{2+}) to the less toxic (and volatile) elemental form, Hg^0. Although detailed information concerning the structure-function relationships of MerA is available (9–12), and comprehensive studies on the distribution and evolution of the enzyme in different nonhypersaline habitats have been published (13, 14), little is known about the molecular adaptations that enable the enzyme to operate in high-salt environments.

Microorganisms have developed two main strategies to ensure that the osmotic pressure of the cytoplasm remains at or above that of the surrounding medium (15). The "salt-in" approach involves the intracellular accumulation of KCl to near-saturation levels (16–19). Obviously, in this case, the cell's proteome and metabolism must be adapted to such high salt concentrations. In general, proteins adapted for function in high-salt environments tend to have large numbers of acidic amino acids and reduced areas of hydrophobic contact surface. At low salt concentration, these halophilic proteins and enzymes usually do not fold correctly and are inactive (20–22).

Microorganisms that utilize the alternative approach actively exclude salt from the cell and synthesize and accumulate organic osmolytes (compatible solutes) in the cytoplasm to maintain osmotic balance (23, 24). A long list of organic solutes has been identified in these species, the most prominent being amino acids, sugars, and their derivatives (23, 24).

We recently characterized a PCR-based MerA from environmental DNA isolated from the microbial community in the lower convective layer (LCL) of the Atlantis II (ATII) brine pool (25). The ATII-LCL MerA is activated by NaCl and exhibits maximum activity at 4.0 M NaCl, indicating that it has evolved to mediate the detoxification of mercury in a salt-in bacterium.

In contrast to the ATII-LCL enzyme, an ortholog from a soil bacterium (26) was found to be inhibited by high NaCl, although the two enzymes differed in sequence by less than 10%. The limited number of structural substitutions observed in ATII-LCL MerA, which must account for its notable activation and catalytic stability in nearly saturated NaCl solutions, makes it an excellent model with which to study the evolution and adaptation of enzymes to hypersaline environments.

In this work, we set out to explore the range of bacterial MerA types found in the hypersaline and mercury-containing environment of the Kebrit brine pool, focusing in particular on the selective impacts of the two osmotic balancing mechanisms. To do so, we have established a PCR-based MerA library using environmental DNA isolated from Kebrit's microbial community and bacterial MerA-specific oligonucleotides as primers. Here, we describe the presence of two catalytically different forms of MerA obtained in the same hypersaline environment. The results shed light on the distinct molecular

Downloaded from http://aem.asm.org/ on August 29, 2020 by guest

adaptations that have evolved to permit the detoxification of mercury in hypersaline environments.

RESULTS AND DISCUSSION

The microbial communities at Kebrit must cope with both the high salt concentration and the presence of heavy metals (27, 28). Hence, they can be expected to (i) make use of the two known mechanisms for the maintenance of cytoplasmic osmotic pressure within the limits imposed by the hypersaline medium (15), and (ii) possess an effective detoxification system for mercury compounds. The structure and properties of MerA enzymes in the Kebrit Deep should therefore reflect the mode of osmotic pressure regulation (salt-in or compatible solutes) used by their respective hosts. In addition, detailed information on the range of structural variation between different MerA enzymes from the microbial community in this environment may also shed light on the evolution of proteins adapted to each of the two osmotic balancing systems. To address these questions, we chose to characterize the sequences and properties of a representative set of PCR-derived bacterial MerA isoforms generated from environmental DNA obtained at Kebrit Deep.

Cloning of MerA genes from Kebrit Deep. Amplification of the different bacterial MerA isoforms from Kebrit environmental DNA is described in Materials and Methods. The product of the amplification process shows a single band of the expected size (1.6 kb) required to encode full-length bacterial MerA enzymes (see Fig. S1B in the supplemental material). The amplified DNA fragment was ligated into the TOPO TA Cloning vector (Invitrogen) and cloned, and a library of Kebrit environmental MerA genes was established.

Sequence analyses of isoforms of MerA present in the bacterial community at Kebrit Deep. The nucleotide sequences of 28 clones from the Kebrit environmental MerA gene library are presented in Fig. S2. Analysis of the sequenced isoforms shows clear structural differences between most of them. Pairwise comparisons of the 28 amino acid sequences show that 27 isoforms display limited amounts of variation, involving a maximum of five residues (shown in red in Fig. S2). Isoform K35 was found to be identical in sequence to the well-characterized MerA enzyme encoded by the *mer* operon on the Tn*501* transposon (29), and it showed the greatest similarity to 26 of the sequences recovered from Kebrit Deep. This isoform was chosen as the standard for comparisons and was named K35NH. The only sequence that shows more substantial sequence divergence from K35NH was isoform K09. This enzyme has 38 amino acid substitutions (relative to K35NH) and was named K09H (Fig. S2).

It is pertinent to note that only two of the 28 sequenced MerA isoforms, K24 and K42, were found to have identical amino acid sequences, differing in two positions from K35NH, with arginine 14 in place of cysteine (see below) and serine 209 in place of glycine. However, within the 27 isoforms represented in the set, 59 amino acid substitutions were identified and were distributed along the entire length of the coding sequence. Some of these substitutions recur in different isoforms. This result indicates the range of diversity within the major bacterial MerA isoforms recovered from Kebrit Deep.

The functional mercuric reductase enzyme is a homodimer, in which each monomer has a catalytic pair of redox-active cysteines, Cys136/Cys141, located in the active site where reduction of the metal ion takes place (11, 12). A second disulfide link, Cys558/Cys559, near the C terminus of each subunit, binds and transfers Hg^{2+} to the active site in the opposite subunit (11, 12). The enzyme also has additional pair of cysteines, Cys11/Cys14, which is part of the conserved metal-binding GMTCXXC sequence located in the N-terminal domain (NmerA) (12). Although the NmerA cysteines have been shown to be dispensable for normal detoxification *in vivo* (12), under physiological conditions in which intracellular thiols are depleted, this pair serves to transfer Hg^{2+} from ligands in the cytoplasm to the catalytic site (10).

Strikingly, in the proteins encoded by 17% of the clones examined (isoforms K02, K24/42, K27, and K34), Cys14 is replaced by arginine. This strongly suggests that the

Downloaded from http://aem.asm.org/ on August 29, 2020 by guest

bacterial populations which harbor these isoforms are able to reduce Hg^{2+} and proceed with the detoxification process only under conditions in which thiols are available in the cell. In this regard, it is worth noting that the Kebrit environment is characterized by a high concentration of H_2S (3). Hydrogen sulfide has been shown to mediate several physiological effects in eukaryotic cells (30, 31), including the promotion of glutathione production (32). In prokaryotic cells, it has been shown that reduced glutathione mediates resistance to H_2S toxicity in oral streptococci (33). Hence, intracellular thiols are likely to be abundant in Kebrit's microorganisms. This in turn would explain why there might be less selective pressure to retain the metal-binding motif within the NmerA domain in this environment. Conversely, environments in which intracellular thiols are limited should select for MerA molecules with a functional metal-binding motif in the NmerA domain to enable delivery of Hg^{2+} to the active site. This observation is supported by our finding that all of 40 clones randomly selected from a PCR-based MerA library established for the microbial community in the Atlantis II brine pool encode the functional Cys11/Cys14 pair in the NmerA domain.

Another substitution that would be expected to affect the activity of the enzyme is observed in K07, in which cysteine 558 is substituted by tyrosine. As mentioned above, the pair of Cys558/Cys559 binds and transfers Hg^{2+} to the active site, and its substitution by alanine resulted in a MerA enzyme that is defective for $HgCl_2$ resistance *in vivo* and reduction of Hg^{2+} *in vitro* (11, 12). Hence, the K07 isoform is most probably inactive and unable to detoxify Hg^{2+}.

The clear distinction between the amino acid sequences of K09H and the K35NH-like isoforms strongly suggests that the two types differ in their catalytic properties, particularly with regard to their responses to NaCl concentration. Figure 1 shows the sequence alignment of MerA K09H with its K35NH orthologs. Both isoforms are 561 amino acids long and retain the three cysteine disulfide pairs involved in the binding of Hg^{2+} (at the C terminus and in the NmerA domain) and its reduction at the catalytic site. The two polypeptide chains are 93% identical. All 38 amino acid substitutions observed in K09H (relative to K35NH) are located in the N-terminal half of the polypeptide chain, specifically within the first 303 amino acids (Fig. 1). The differences can be summarized as follows. Relative to K35NH, K09H shows an overall gain of three serine and two aspartic acid residues and one each of glutamic acid, threonine, cysteine, glutamine, methionine, isoleucine, leucine, and histidine. Conversely, it has lost three alanines and prolines, two each of valine, asparagine, and lysine, and one arginine (Fig. S3A). Functional classification of amino acids that differentiate K09H from the K35NH orthologs reveals an increase in acidic and uncharged polar side chains at the expense of hydrophobic amino acids (Fig. S3B). These features indicate that the K09H and K35NH orthologs are adapted for function in high and low salt concentrations, respectively (20–22).

For phylogenetic analyses of K09H and K35NH, we determined that sequence K35NH was identical (100% amino acid identity) to more than 170 other sequences available in GenBank from various species, including the well-characterized MerA enzyme encoded by the *mer* operon on the Tn*501* transposon (29). We speculate that this transposon has enabled this gene to be horizontally transferred between the genomes of many different bacteria. MerAs with amino acid sequences identical to that of K35NH are found in five different genera of *Betaproteobacteria* and seven genera of the *Gammaproteobacteria*, as well as in one genus (*Bacillus*) in the phylum *Firmicutes*. In terms of nucleotide sequence, the K35NH gene is 97% identical to homologs from five betaproteobacteria and three gammaproteobacteria, which are 100% identical to each other. These results suggest that the K35NH sequence described here originated from a betaproteobacterium or a gammaproteobacterium. A more precise phylogenetic assessment will require amplification and sequencing of a larger genomic fragment that includes K35NH.

In the case of K09H, the phylogenetic results are, at first sight, more informative. The amino acid sequence of K09H differs from that of its top BLASTP hit, and this enabled us to construct a phylogenetic tree including the 20 best hits with a defined species of

Downloaded from http://aem.asm.org/ on August 29, 2020 by guest

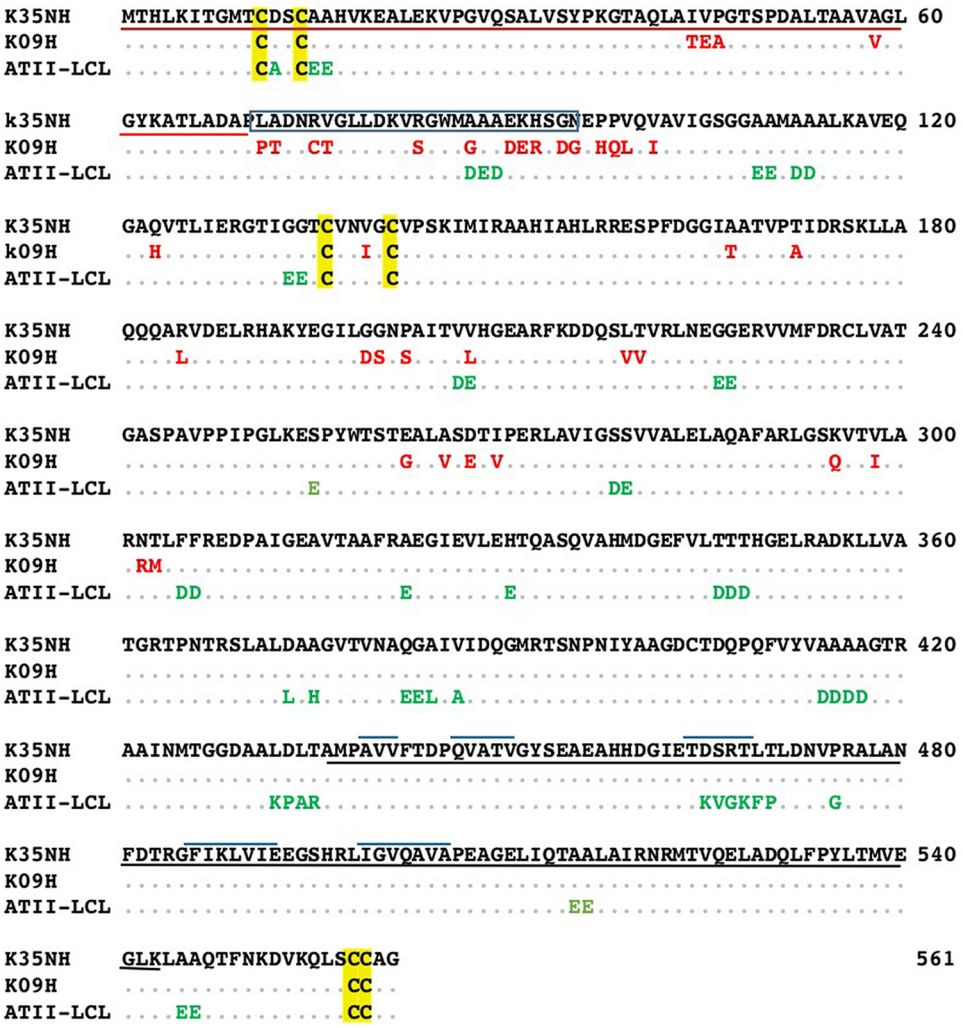

FIG 1 Alignment of the sequences of the MerA enzymes K35NH, K09H, and ATII-LCL. Amino acid positions in K09H and ATII-LCL that differ from their counterparts in K35NH (the uppermost sequence) are highlighted in red and green, respectively. Dots refer to residues that are identical to those in K35NH. Cysteine pairs in the NmerA domain (Cys11/Cys14) and near the C terminus (Cys558/Cys559) that are involved in binding of Hg^{2+} and the pair of cysteines required for the reduction of Hg^{2+} (Cys136/Cys141) are highlighted in yellow (11, 12). The NmerA domain, the dimerization domain, and β-strand structures present in the dimerization domain are underlined in red and black and overlined in blue, respectively. The boxed amino acids between the NmerA domain and the catalytic domain (amino acids 70 to 95) are not included in the 3D structures presented in Fig. 4.

origin (Fig. S4). All of these hits were either betaproteobacteria or gammaproteobacteria. Nucleotide sequence comparison between the K09H gene and that of its closest BLASTP hit, a gene belonging to *Acidovorax* sp. strain GW101-3H11, revealed 95% identity. However, tempting though it may be to hypothesize that K09H belongs to a close relative of *Acidovorax*, the results we obtained for K35NH show that the K09H gene may also have undergone horizontal transfer. Hence, the similarity to the *Acidovorax* gene cannot be taken as reliable evidence on which to base a phylogenetic assignment. Here, too, a more precise identification will require the recovery and sequencing of a larger genomic fragment.

Effects of high NaCl concentration on the activities of MerA K09H and its ortholog K35NH. To determine whether the two types of MerAs respond differently to salt (as implied by the indicated sequence differences between them), we expressed and compared the activities of the products of the corresponding PCR-derived genes. The coding sequences for K35NH and K09H were cloned into the pET-SUMO expression vector (Invitrogen) and expressed in *E. coli*, and the recombinant enzymes were purified

Downloaded from http://aem.asm.org/ on August 29, 2020 by guest

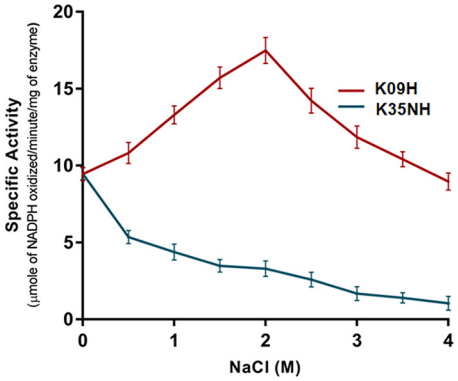

FIG 2 Effect of NaCl concentration on the activity of K35NH and K09H. The enzymes were assayed in reaction mixture containing the indicated concentration of NaCl. For details of the assay, see Materials and Methods.

using HisTrap affinity column. Details of the induction and purification process are described in Materials and Methods. Analysis of the purified enzymes by SDS-PAGE is presented in Fig. S5.

To examine if and how the amino acid differences between K09H and K35NH affect their responses to salt, we measured the activities of the purified enzymes in the presence of various concentrations of NaCl. Figure 2 shows the catalytic properties of both isoforms in the presence of increasing concentrations of NaCl. K35NH is strongly inhibited by NaCl, retaining 36% and 13.7% of its maximum activity (in the absence of NaCl) at concentrations of 2.0 M and 4.0 M NaCl, respectively. In contrast, the K09H ortholog is activated by NaCl, reaching its maximum activity at 2.0 M NaCl, an increase of 1.8-fold relative to its activity in the absence of NaCl. Thus, K09H is at least 5.8-fold more active than K35NH under these conditions. At NaCl concentrations higher than 2.0 M, K09H activity decreases steadily, but it is nevertheless 6.8-fold more active than K35NH at 4.0 M NaCl.

This result shows that (at least) two catalytically different bacterial forms of MerA are represented in the highly saline environment of Kebrit Deep. One is strongly inhibited by NaCl, while the other is activated in an NaCl-dependent manner. The intracellular KCl concentration in microorganisms that utilize the salt-in approach has been estimated to be around 4.0 M (15, 16, 18, 34). It could therefore be argued that K09H, with its maximum activity at 2.0 M, could not support the detoxification process in a salt-in organism. However, it is important to note that MerA K09H retains considerably more activity in 4.0 M NaCl than does K35NH, which is virtually inactive under the same conditions. The specific activity of K09H at 4.0 M NaCl is 8.9 μmol NADPH oxidized per min per mg of enzyme, which is most probably enough to support Hg^{2+} detoxification via reduction *in vivo* at 4 M NaCl. Hence, the structures and responses of these two orthologs to NaCl concentration indicate that they probably evolved in bacterial microorganisms that exploit distinct approaches to cope with their hypersaline environments, with K09H utilizing the salt-in strategy and K35NH the compatible-solutes mode.

It has been reported that archaeal MerAs lack the NmerA domain (14). The oligonucleotide primers used to construct the MerA gene library in this work were based on the transposon Tn*501* and bacterial MerA sequences that include the NmerA domain. Therefore, this primer pair would not be expected to amplify MerA from archaeal microorganisms. We therefore assume that K35NH and K09H originated from bacterial microorganisms harboring MerA sequences that had once been acquired through horizontal gene transfer of the transposon Tn*501* and were subsequently adapted to the hypersaline environment of Kebrit Deep.

The 28 Kebrit MerA sequences reported in this work were generated from clones selected randomly from our PCR-based MerA library. Only one, K09H, showed a

Downloaded from http://aem.asm.org/ on August 29, 2020 by guest

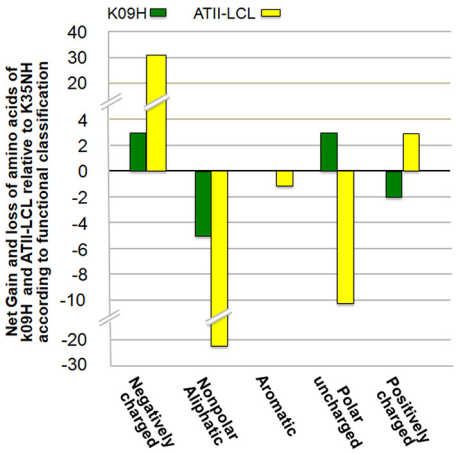

FIG 3 Profile of gains and losses of amino acids belonging to the indicated functional classes for K09H and ATII-LCL relative to K35NH. For suitable comparison, the net changes in numbers of amino acids of the indicated functional class in K09H and ATII-LCL relative to K35NH are presented together. The data for K09H were obtained from Fig. S3B, while those for ATII-LCL are adapted from reference 25 (© the American Society for Biochemistry and Molecular Biology).

halophilic signature, with a prevalence of acidic amino acids at the expense of hydrophobic residues, and is activated by salt, while the other 27 sequences, including K35NH, have no halophilic signature, and K35NH itself is inhibited by NaCl. The MerA diversity noted in this work most probably reflects the fraction of bacterial MerA enzymes that possess the NmerA domain and whose nucleotide sequences match the primers used in the amplification process (which are derived from the *merA* gene in the operon carried by the transposon Tn*501*). Interestingly, the low abundance of MerA with a halophilic signature observed in this work is compatible with the previously reported low incidence of the salt-in approach in halophilic microorganisms (35).

It is interesting to note that although most extreme halophiles that use the salt-in strategy are members of the domain Archaea (36), the use of KCl as an osmoprotectant has also been reported for the halophilic gammaproteobacterium *Halorhodospira halophila* (34). The fact that a salt-in strategy was described for a bacterium belonging to the *Gammaproteobacteria* is compatible with our preliminary phylogenetic classification of K09H.

Structural and NaCl activation differences between K09H and ATII-LCL. The profile of the salt-dependent activation of K09H differs somewhat from that of the halophilic MerA ATII-LCL reported previously from the Atlantis II brine pool (25). Although both enzymes are activated by NaCl, MerA K09H reaches its maximum activity at 2.0 M NaCl, while the MerA ATII-LCL displays maximum activity at 4.0 M NaCl (25). Interestingly, although the orthologous enzymes ATII-LCL and K09H are activated in a salt concentration-dependent manner, the amino acid substitutions that differentiate them from the salt-sensitive isoform K35NH are quite distinct from each other. Indeed, none of them is shared by both proteins (compare substitutions highlighted in red [K09H] and green [ATII-LCL] in Fig. 1). What the two halophilic orthologs do have in common in this context is the functional classification of the substitutions that distinguish them from the nonhalophilic ortholog K35NH, which results in an increase in acidic amino acids and a decrease in the number of nonpolar aliphatic side chains (Fig. 3). As mentioned above, this feature is characteristic of enzymes that are stable and catalytically active at high salt concentration (20–22). Furthermore, ATII-LCL has substantially more of both categories of amino acids than K09H (Fig. 3). The relative increase of these critical amino acids in ATII-LCL, in comparison to K09H, may account for the superior stability of ATII-LCL at 4.0 M NaCl.

Distribution of amino acid substitutions in the three-dimensional structure of K09H. The K09H catalytic core and its N-terminal domain sequences were subjected to

Downloaded from http://aem.asm.org/ on August 29, 2020 by guest

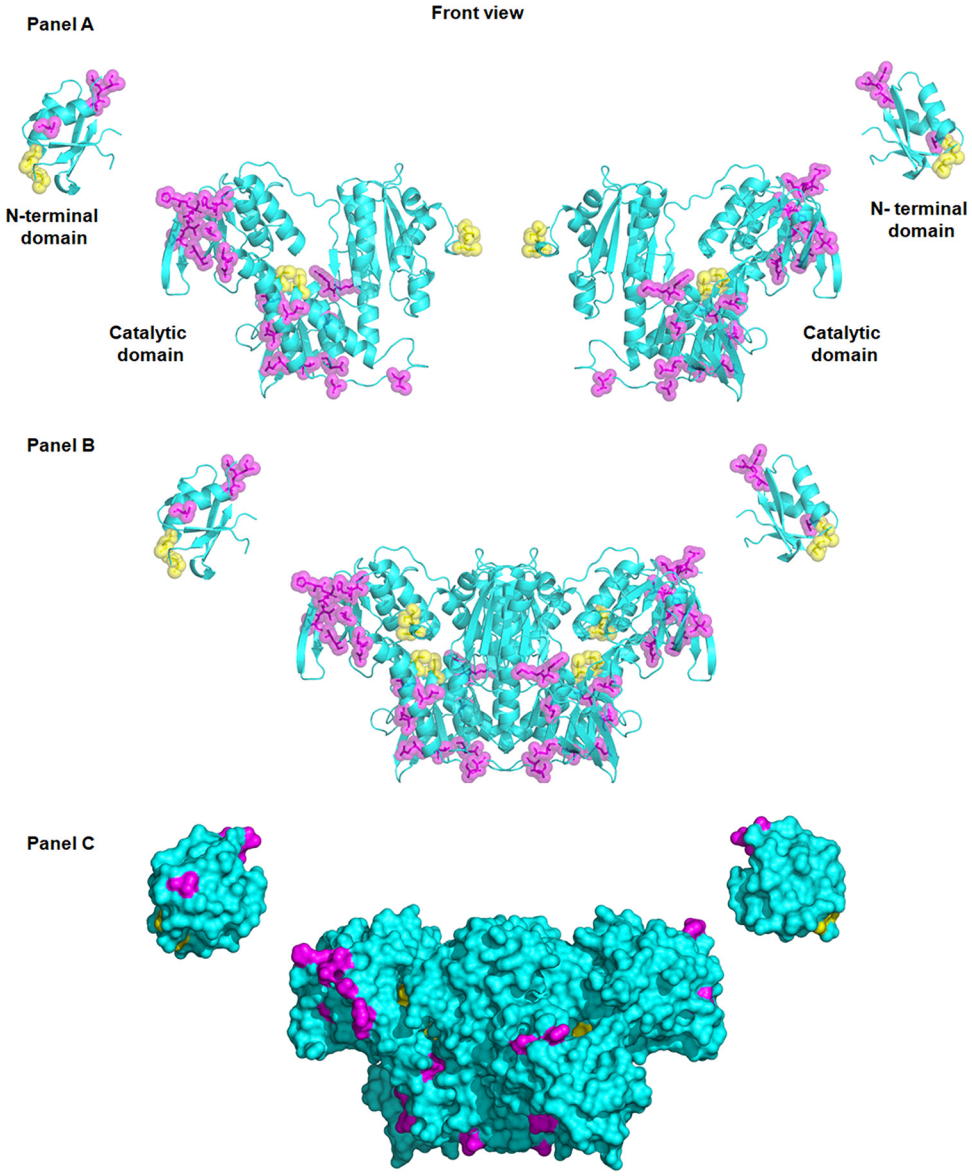

FIG 4 Homology modeling of the three-dimensional structure of the homodimer K09H based on Tn*501* MerA. Modeling of the N-terminal and catalytic domains of MerA K09H is based on the Tn*501* enzyme (9, 10) and was performed as described in Materials and Methods. (A) Ribbon diagram of the 3D structure of the two identical subunits. (B) Homodimer ribbon model in which the two subunits interact via their dimerization domains. (C) Space-filling model of the homodimer shown in panel B. Yellow spheres represent the cysteines that participate in Hg^{2+} binding and reduction; amino acids shown in purple in panels A and B are those that substitute for the residues in corresponding positions in K35NH, while the purple amino acids in the space-filling model are those that are found on the surface of the molecule. In panels A to C, the model is viewed from the front. The top view of the 3D model is shown in Fig. S7. The five antiparallel β-sheets present in the dimerization domain are shown in Fig. S6. None of the available structures include the 25 residues that link the N-terminal domain to the catalytic domain (boxed in Fig. 1).

homology modeling against Tn*501* MerA (9, 10). The model presented in Fig. 4 shows the identical monomers (Fig. 4A) and the homodimeric structure of the enzyme (Fig. 4B). The three-dimensional (3D) structure of the 25-residue linker (positions 70 to 95, boxed in Fig. 1) that connects the N-terminal domain with the catalytic core has not been determined and is not included in Fig. 4. MerA has five β-strands (overlined in blue in Fig. 1; see also Fig. S6) within its dimerization domain (underlined in black in Fig. 1), which is conserved among the family of homodimeric pyridine nucleotide-disulfide oxidoreductases (37). It is interesting to note that all the substitutions observed in K09H

Downloaded from http://aem.asm.org/ on August 29, 2020 by guest

are located outside this domain (Fig. 4A and B). A plausible explanation for this observation is that MerA functions as a dimer, in which the cysteine pair 558/559 in one subunit binds Hg^{2+} and transfers the ion to cysteines 136/141 in the active site of the other subunit (11, 12). Spontaneous mutations in the dimerization domain could then interfere with the dimerization process and with enzyme function. In environments in which levels of mercury are high, microorganisms harboring such mutations will be subject to negative selection.

The amino acid substitutions located on the surface of the dimer are also shown in Fig. 4C (see also Fig. S7). Of the 38 substitutions found in K09H, 10 are located within the 25-residue stretch that connects the NmerA domain with the catalytic domain. The remaining 28 substitutions map to the NmerA and catalytic domains, and 26 substitutions were found to be located on the surface of the enzyme. The two that are buried in the molecule are Val219 and Ile298. Based on the homology model, none of the 28 amino acid substitutions in the NmerA and catalytic domains are in a position to form ionic bonds. Therefore, most probably, the stability and activation conferred on K09H in the presence of high concentrations of salt are due to the decrease in the total area of the hydrophobic contact surface (38).

This work highlights several aspects of the molecular evolution of mercuric reductases in bacterial microbial communities that live in two hypersaline brine pools, Kebrit and Atlantis II, in the Red Sea. The results show that two catalytically and structurally different isoforms of MerA occur at Kebrit Deep for detoxification of mercuric compounds. One is inhibited and the other activated by elevated concentrations of NaCl. These two isoforms may well be expressed by bacterial microorganisms that use the compatible solutes and the salt-in mechanisms, respectively, to survive in their hypersaline environment.

MATERIALS AND METHODS

Collection of water samples and isolation of environmental DNA from the Kebrit brine pool. Water samples were collected during the Red Sea expedition undertaken during the King Abdullah University for Sciences and Technology (KAUST; Thuwal, Kingdom of Saudi Arabia) oceanographic cruise of the R/V *Aegaeo* in March/April 2010. Around 120 liters of water samples was collected from Kebrit brine (24°44′N, 36°17′E) at 1,490 m below the surface, using Niskin bottles connected to conductivity, temperature, and depth sensors (CTDs).

Microorganisms in these samples were then divided into individual size classes by sequential filtration through Millipore 293-mm cellulose filters (nitrocellulose/cellulose acetate), with pore sizes of 3 μm, 0.8 μm, and 0.1 μm, using stainless steel filter holders. Filters were stored in sucrose lysis buffer at −20°C and transported to the laboratory at the American University in Cairo for processing.

Construction of a MerA gene library for the Kebrit Deep microbial community. Environmental DNA was isolated from the microbial community trapped on the 0.1-μm filter, using a metagenomic DNA isolation kit for water-sourced samples (Epicentre).

The gene library was established by amplification of sequences encoding MerA enzymes, using a pair of MerA-specific oligonucleotides as primers and environmental DNA Kebrit as the template. The MerA primers were designed on the basis of two publicly available MerA sequences obtained from an uncultured soil bacterium (26) and the transposon Tn*501* (29), respectively. Alignment of these MerA sequences shows that their 5′ and 3′ ends have identical nucleotide sequences. In addition, the primer sequences were identical to the corresponding parts of the consensus sequence of the assembled ATII-LCL MerA reads generated from an ATII-LCL metagenomic data set based on 454 pyrosequencing (25). The MerA-specific oligonucleotides used here have the following sequences: forward primer, 5′-ATGACCCATCTAAAAATCACCGGCATGACTTG-3′; and reverse primer, 3′-GAAGCAGCTTTCCTGCTGCGCC GGGTGA-5′ (see Fig. S1A). PCR was performed for 25 cycles of 95°C for 30 s (denaturation), 30 s at 68°C (annealing), and 72°C for 90 s (extension), followed by a final extension for 7 min at 72°C. The amplified DNA fragment was then cloned into the TOPO-TA Cloning vector (Invitrogen). Clones were selected randomly and sequenced in both directions using the Sanger dideoxy method.

It is important to note that the average Phred base-specific quality score for the total set of DNA sequences was 16, and 95% of the bases scored >20, indicating that the sequences obtained were all of high quality. In addition, we used Phusion high-fidelity DNA polymerase, whose error frequencies typically lie in the range of 10^{-6} mutations/bp amplified (39). Therefore, we believe that the amino acid substitutions observed in the MerA sequences reported in this work are most probably genuine and hence accurately represent the different MerA isoforms in the bacterial community of the Kebrit brine pool environment.

Primary structure analysis. Alignment of MerA sequences was performed using the STRuctural Alignment of Proteins (STRAP) editor (40). The pyridine nucleotide-disulfide oxidoreductase dimerization domain (P-code PF02852.17) of MerAs was identified by performing an HMMScan search of their amino acid sequences against the Pfam-A database (version 27.0) (41) on the HMMER Web server (42).

Downloaded from http://aem.asm.org/ on August 29, 2020 by guest

Expression and purification of recombinant MerA enzymes. The coding sequences of the *merA* genes were subcloned into the Champion pET-SUMO expression vector. MerA recombinant proteins were expressed in *E. coli* BL21(DE3) cells, and the enzymes were purified as described before (25). Briefly, transformed cell cultures supplemented with 20 μM flavin adenine dinucleotide (FAD) were induced with 1 mM isopropyl β-D-thiogalactoside at an A_{600} of 0.5 for 3 h and then lysed in TE buffer (10 mM Tris-HCl [pH 7.5], containing 1 mM EDTA) supplemented with 20 μM FAD. After the removal of insoluble debris by centrifugation, the supernatants were purified on HisTrap columns (Amersham Biosciences), as described before (25). Protein purity was assessed by electrophoresis on 12% SDS-polyacrylamide gels.

Enzyme assay. Mercuric reductase assays were performed at 25°C in 80 mM sodium phosphate buffer (pH 7.4) containing 100 μM NADPH, 50 μM $HgCl_2$, and 1 mM β-mercaptoethanol in a final volume of 1 ml. The reaction was started by the addition of NADPH, and the enzyme activity was determined by monitoring the initial rate of NADPH oxidation at 340 nm using a Shimadzu UV-1800 spectrophotometer. One unit of mercuric reductase activity was defined as the amount of enzyme that catalyzes the Hg^{2+}-dependent oxidation of 1 μmol NADPH/min (43). For NaCl-dependent activation or inhibition, the enzyme activity was measured in the presence of the indicated concentrations of NaCl.

Phylogenetic analysis. For the similarity and phylogenetic analysis of sequences, K35NH and K09H we searched the GenBank NR database using BLASTP. For nucleotide sequence comparison, we used BLASTN (44).

For K09H, we reconstructed a phylogenetic tree using IQ-TREE (45) on the IQ-TREE Web server with default parameter values. The sequences used in the reconstruction were a selection of the NR best hits returned by BLASTP. We used as a criterion for hit selection that the hit should be associated with a defined species (as opposed to "uncultured organism") and that its genus should not repeat that from an already-selected sequence. The sequences selected are given in Table S1.

Modeling the three-dimensional structure of K09H MerA. The three-dimensional structure of the K09H MerA was predicted using SWISS-MODEL homology modeling (46–48) against the N-terminal (PDB 2KT2) (9) and C-terminal (PDB 1ZK7) (10) domains of the Tn*501* mercuric reductase (GenBank accession number CAA77323). For identification of the surface residues, the plug-in script "findSurfaceResidues.py" (https://github.com/Pymol-Scripts/Pymol-script-repo/blob/master/findSurfaceResidues.py) in the PyMOL molecular graphics system (version 1.7.2.1; Schrödinger, LLC) was used. Labeling of the active-site residues and amino acid substitutions, superposition of the N- and C-terminal models of K09H MerA, and rendering of the final 3D structural models and surface images were performed using PyMOL.

Accession number(s). The nucleotide sequence(s) reported in this paper has been submitted to the GenBank/EBI Data Bank with accession numbers KY421641 to KY421666 (see Table S2 in the supplemental material).

SUPPLEMENTAL MATERIAL

Supplemental material for this article may be found at https://doi.org/10.1128/AEM.01431-18.

SUPPLEMENTAL FILE 1, PDF file, 1.9 MB.

ACKNOWLEDGMENTS

We are grateful to Paul Hardy for critical reading of the manuscript.

This work was supported by an AUC internal grant.

We declare no conflicts of interest with the contents of this article.

E.R., M.M. and H.E.D. conceived and designed the experiments; E.R. and M.M. performed the experiments; A.E.H., E.R., F.S.C., J.C.S., and M.M. analyzed the data computationally; and H.E.D. wrote the paper.

REFERENCES

1. Antunes A, Ngugi DK, Stingl U. 2011. Microbiology of the Red Sea (and other) deep-sea anoxic brine lakes. Environ Microbiol Rep 3:416–433. https://doi.org/10.1111/j.1758-2229.2011.00264.x.
2. Backer H, Schoell M. 1972. New deeps with brines and metalliferous sediments in the Red Sea. Nat Phys Sci 240:153–158. https://doi.org/10.1038/physci240153a0.
3. Hartmann M, Scholten JC, Stoffers P, Wehner F. 1998. Hydrographic structure of brine-filled Deeps in the Red Sea—new results from the Shaban, Kebrit, Atlantis II, and Discovery Deep. Mar Geol 144:311–330. https://doi.org/10.1016/S0025-3227(97)00055-8.
4. Swift SA, Bower AS, Schmitt RW. 2012. Vertical, horizontal, and temporal changes in temperature in the Atlantis II and Discovery hot brine pools, Red Sea. Deep Sea Res 164:118–128. https://doi.org/10.1016/j.dsr.2012.02.006.
5. Eder W, Jahnke LL, Schmidt M, Huber R. 2001. Microbial diversity of the brine-seawater interface of the Kebrit Deep, Red Sea, studied via 16S rRNA gene sequences and cultivation methods. Appl Environ Microbiol 67:3077–3085. https://doi.org/10.1128/AEM.67.7.3077-3085.2001.
6. Eder W, Ludwig W, Huber R. 1999. Novel 16S rRNA gene sequences retrieved from highly saline brine sediments of Kebrit Deep, Red Sea. Arch Microbiol 172:213–218.
7. Freedman Z, Zhu C, Barkay T. 2012. Mercury resistance and mercuric reductase activities and expression among chemotrophic thermophilic Aquificae. Appl Environ Microbiol 78:6568–6575. https://doi.org/10.1128/AEM.01060-12.
8. Barkay T, Wagner DI. 2005. Microbial transformations of mercury: potentials, challenges, and achievements in controlling mercury toxicity in the environment. Adv Appl Microbiol 57:1–52. https://doi.org/10.1016/S0065-2164(05)57001-1.
9. Ledwidge R, Hong B, Dotsch V, Miller SM. 2010. NmerA of Tn501 mercuric ion reductase: structural modulation of the pK_a values of the metal binding cysteine thiols. Biochemistry 49:8988–8998. https://doi.org/10.1021/bi100537f.
10. Ledwidge R, Patel B, Dong A, Fiedler D, Falkowski M, Zelikova J, Summers AO, Pai EF, Miller SM. 2005. NmerA, the metal binding domain of

Downloaded from http://aem.asm.org/ on August 29, 2020 by guest

mercuric ion reductase, removes Hg^{2+} from proteins, delivers it to the catalytic core, and protects cells under glutathione-depleted conditions. Biochemistry 44:11402–11416. https://doi.org/10.1021/bi050519d.
11. Miller SM, Moore MJ, Massey V, Williams CH, Jr, Distefano MD, Ballou DP, Walsh CT. 1989. Evidence for the participation of Cys558 and Cys559 at the active site of mercuric reductase. Biochemistry 28:1194–1205.
12. Moore MJ, Walsh CT. 1989. Mutagenesis of the N- and C-terminal cysteine pairs of Tn501 mercuric ion reductase: consequences for bacterial detoxification of mercurials. Biochemistry 28:1183–1194. https://doi.org/10.1021/bi00429a036.
13. Oregaard G, Sorensen SJ. 2007. High diversity of bacterial mercuric reductase genes from surface and sub-surface floodplain soil (Oak Ridge, USA). ISME J 1:453–467. https://doi.org/10.1038/ismej.2007.56.
14. Simbahan J, Kurth E, Schelert J, Dillman A, Moriyama E, Jovanovich S, Blum P. 2005. Community analysis of a mercury hot spring supports occurrence of domain-specific forms of mercuric reductase. Appl Environ Microbiol 71:8836–8845. https://doi.org/10.1128/AEM.71.12.8836-8845.2005.
15. Oren A. 2008. Microbial life at high salt concentrations: phylogenetic and metabolic diversity. Saline Syst 4:2. https://doi.org/10.1186/1746-1448-4-2.
16. Christian JH, Waltho JA. 1962. Solute concentrations within cells of halophilic and non-halophilic bacteria. Biochim Biophys Acta 65:506–508.
17. Eisenberg H, Mevarech M, Zaccai G. 1992. Biochemical, structural, and molecular genetic aspects of halophilism. Adv Protein Chem 43:1–62.
18. Lanyi JK. 1974. Salt-dependent properties of proteins from extremely halophilic bacteria. Bacteriol Rev 38:272–290.
19. Oren A, Heldal M, Norland S, Galinski EA. 2002. Intracellular ion and organic solute concentrations of the extremely halophilic bacterium Salinibacter ruber. Extremophiles 6:491–498. https://doi.org/10.1007/s00792-002-0286-3.
20. Paul S, Bag SK, Das S, Harvill ET, Dutta C. 2008. Molecular signature of hypersaline adaptation: insights from genome and proteome composition of halophilic prokaryotes. Genome Biol 9:R70. https://doi.org/10.1186/gb-2008-9-4-r70.
21. Fukuchi S, Yoshimune K, Wakayama M, Moriguchi M, Nishikawa K. 2003. Unique amino acid composition of proteins in halophilic bacteria. J Mol Biol 327:347–357.
22. Frolow F, Harel M, Sussman JL, Mevarech M, Shoham M. 1996. Insights into protein adaptation to a saturated salt environment from the crystal structure of a halophilic 2Fe-2S ferredoxin. Nat Struct Biol 3:452–458.
23. Galinski EA. 1986. Osmoadaptation in bacteria. Adv Microb Physiol 37:273–228.
24. Roberts MF. 2005. Organic compatible solutes of halotolerant and halophilic microorganisms. Saline Syst 1:5. https://doi.org/10.1186/1746-1448-1-5.
25. Sayed A, Ghazy MA, Ferreira AJ, Setubal JC, Chambergo FS, Ouf A, Adel M, Dawe AS, Archer JA, Bajic VB, Siam R, El-Dorry H. 2014. A novel mercuric reductase from the unique deep brine environment of Atlantis II in the Red Sea. J Biol Chem 289:1675–1687. https://doi.org/10.1074/jbc.M113.493429.
26. Sen D, Van der Auwera GA, Rogers LM, Thomas CM, Brown CJ, Top EM. 2011. Broad-host-range plasmids from agricultural soils have IncP-1 backbones with diverse accessory genes. Appl Environ Microbiol 77:7975–7983. https://doi.org/10.1128/AEM.05439-11.
27. Bischoff JL. 1969. Red Sea geothermal brine deposits: their mineralogy, chemistry, and genesis, p 368–401. *In* Degens ET, Ross DA (ed), Hot brines and recent heavy metal deposits in the Red Sea: a geochemical and geophysical account. Springer, Berlin, Germany.
28. Scholten JC, Stoffers P, Garbe-Schonberg D, Moammar M. 1999. Hydrothermal mineralization in the Red Sea, p 369–395. *In* Cronan DS (ed), Handbook of marine mineral deposits. CRC Press, Boca Raton, FL.
29. Brown NL, Ford SJ, Pridmore RD, Fritzinger DC. 1983. Nucleotide sequence of a gene from the Pseudomonas transposon Tn501 encoding mercuric reductase. Biochemistry 22:4089–4095.
30. Calvert JW, Coetzee WA, Lefer DJ. 2010. Novel insights into hydrogen sulfide-mediated cytoprotection. Antioxid Redox Signal 12:1203–1217. https://doi.org/10.1089/ars.2009.2882.
31. Li L, Moore PK. 2008. Putative biological roles of hydrogen sulfide in health and disease: a breath of not so fresh air? Trends Pharmacol Sci 29:84–90. https://doi.org/10.1016/j.tips.2007.11.003.
32. Kimura Y, Goto Y, Kimura H. 2010. Hydrogen sulfide increases glutathione production and suppresses oxidative stress in mitochondria. Antioxid Redox Signal 12:1–13. https://doi.org/10.1089/ars.2008.2282.
33. Ooi XJ, Tan KS. 2016. Reduced glutathione mediates resistance to H_2S toxicity in oral streptococci. Appl Environ Microbiol 82:2078–2085. https://doi.org/10.1128/AEM.03946-15.
34. Deole R, Challacombe J, Raiford DW, Hoff WD. 2013. An extremely halophilic proteobacterium combines a highly acidic proteome with a low cytoplasmic potassium content. J Biol Chem 288:581–588. https://doi.org/10.1074/jbc.M112.420505.
35. Oren H. 1999. Bioenergetic aspects of halophilism. Microbiol Mol Biol Rev 63:334–348.
36. Kennedy SP, Ng WV, Salzberg SL, Hood L, DasSarma S. 2001. Understanding the adaptation of Halobacterium species NRC-1 to its extreme environment through computational analysis of its genome sequence. Genome Res 11:1641–1650. https://doi.org/10.1101/gr.190201.
37. Zhang Y, Bond CS, Bailey S, Cunningham ML, Fairlamb AH, Hunter WN. 1996. The crystal structure of trypanothione reductase from the human pathogen Trypanosoma cruzi at 2.3 Å resolution. Protein Sci 5:52–61.
38. Siglioccolo A, Paiardini A, Piscitelli M, Pascarella S. 2011. Structural adaptation of extreme halophilic proteins through decrease of conserved hydrophobic contact surface. BMC Struct Biol 11:50. https://doi.org/10.1186/1472-6807-11-50.
39. McInerney P, Adams P, Hadi MZ. 2014. Error rate comparison during polymerase chain reaction by DNA polymerase. Mol Biol Int 2014:287430. https://doi.org/10.1155/2014/287430.
40. Gille C, Frommel C. 2001. STRAP: editor for STRuctural Alignments of Proteins. Bioinformatics 17:377–378.
41. Punta M, Coggill PC, Eberhardt RY, Mistry J, Tate J, Boursnell C, Pang N, Forslund K, Ceric G, Clements J, Heger A, Holm L, Sonnhammer EL, Eddy SR, Bateman A, Finn RD. 2012. The Pfam protein families database. Nucleic Acids Res 40:D290–D301. https://doi.org/10.1093/nar/gkr1065.
42. Hunter S, Jones P, Mitchell A, Apweiler R, Attwood TK, Bateman A, Bernard T, Binns D, Bork P, Burge S, de Castro E, Coggill P, Corbett M, Das U, Daugherty L, Duquenne L, Finn RD, Fraser M, Gough J, Haft D, Hulo N, Kahn D, Kelly E, Letunic I, Lonsdale D, Lopez R, Madera M, Maslen J, McAnulla C, McDowall J, McMenamin C, Mi H, Mutowo-Muellenet P, Mulder N, Natale D, Orengo C, Pesseat S, Punta M, Quinn AF, Rivoire C, Sangrador-Vegas A, Selengut JD, Sigrist CJ, Scheremetjew M, Tate J, Thimmajanarthanan M, Thomas PD, Wu CH, Yeats C, Yong SY. 2012. InterPro in 2011: new developments in the family and domain prediction database. Nucleic Acids Res 40:D306–D312. https://doi.org/10.1093/nar/gkr948.
43. Fox B, Walsh CT. 1982. Mercuric reductase. Purification and characterization of a transposon-encoded flavoprotein containing an oxidation-reduction-active disulfide. J Biol Chem 257:2498–2503.
44. Altschul SF, Madden TL, Schaffer AA, Zhang J, Zhang Z, Miller W, Lipman DJ. 1997. Gapped BLAST and PSI-BLAST: a new generation of protein database search programs. Nucleic Acids Res 25:3389–3402.
45. Nguyen LT, Schmidt HA, von Haeseler A, Minh BQ. 2015. IQ-TREE: a fast and effective stochastic algorithm for estimating maximum-likelihood phylogenies. Mol Biol Evol 32:268–274. https://doi.org/10.1093/molbev/msu300.
46. Guex N, Peitsch MC. 1997. SWISS-MODEL and the Swiss-PdbViewer: an environment for comparative protein modeling. Electrophoresis 18:2714–2723. https://doi.org/10.1002/elps.1150181505.
47. Arnold K, Bordoli L, Kopp J, Schwede T. 2006. The SWISS-MODEL workspace: a web-based environment for protein structure homology modelling. Bioinformatics 22:195–201. https://doi.org/10.1093/bioinformatics/bti770.
48. Schwede T, Kopp J, Guex N, Peitsch MC. 2003. SWISS-MODEL: an automated protein homology-modeling server. Nucleic Acids Res 31:3381–3385.

Downloaded from http://aem.asm.org/ on August 29, 2020 by guest